

Article

Efficient Removal of Cr(VI) by Protonated Amino-Bamboo Char Prepared via Radiation Grafting: Behavior and Mechanism

Yuan Zhao ^{1,†} , Jie Gao ^{1,†}, Tian Liang ¹, Tao Chen ^{1,*} , Xiaobing Han ¹ , Guowen Hu ¹ and Bing Li ^{2,*}

¹ Hubei Key Laboratory of Radiation Chemistry and Functional Materials, School of Nuclear Technology and Chemistry & Biology, Hubei University of Science and Technology, Xianning 437100, China; zhyf308@hust.edu.cn (Y.Z.); gaojie2019@hust.edu.cn (J.G.); new.tony.leung.3@gmail.com (T.L.); hanxiaobing@hust.edu.cn (X.H.); hgwpublish@163.com (G.H.)

² College of Chemistry and Materials Engineering, Zhejiang A&F University, Hangzhou 311300, China

* Correspondence: taochen518@163.com (T.C.); libingzjfc@163.com (B.L.)

† These authors contributed equally to this work.

Abstract: Biochar is considered to be the most promising substrate for the preparation of environmentally functional materials. The modification of bamboo char can significantly improve the removal rate of toxic ions from wastewater; however, there are few reports that focus on the radiation grafting method. Here, glyceride methacrylate (GMA) is successfully grafted onto bamboo char through electron beam radiation, followed by amination using the existing epoxide group in diethyltriamine, and finally, treated with hydrochloric acid to obtain protonated diethyltriamine-functionalized bamboo char (CDGBC). The results of IR, TG, XRD, and SEM prove the successful fabrication of a CDGBC biosorbent. The results show that the solution pH has a great effect on the adsorption capacity, and a maximum adsorption capacity of 169.13 mg/g is obtained at pH = 2 for Cr(VI). In addition, the adsorption behavior of Cr(VI) onto CDGBC is demonstrated to obey the pseudo-second-order kinetic and Freundlich isotherm models, and thermodynamic analysis exhibits that Cr(VI) adsorption is an endothermic spontaneous process. A possible adsorption mechanism based on the electrostatic interaction, reduction, and surface complexation is proposed, according to the obtained results. This work confirms that radiation-induced grafting modification can effectively transform biochar into a high-performance adsorbent for Cr(VI) removal, offering a new approach to synthesizing an efficient biosorbent.

Keywords: bamboo char; radiation-induced grafting; Cr(VI); adsorption; mechanism



Citation: Zhao, Y.; Gao, J.; Liang, T.; Chen, T.; Han, X.; Hu, G.; Li, B. Efficient Removal of Cr(VI) by Protonated Amino-Bamboo Char Prepared via Radiation Grafting: Behavior and Mechanism. *Sustainability* **2023**, *15*, 13560. <https://doi.org/10.3390/su151813560>

Academic Editor: Chenggang Gu

Received: 25 June 2023

Revised: 29 August 2023

Accepted: 29 August 2023

Published: 11 September 2023



Copyright: © 2023 by the authors. Licensee MDPI, Basel, Switzerland. This article is an open access article distributed under the terms and conditions of the Creative Commons Attribution (CC BY) license (<https://creativecommons.org/licenses/by/4.0/>).

1. Introduction

In recent years, heavy metal pollution caused by industrial and agricultural activity has attracted extensive attention. Compared with organic pollutants, inorganic pollutants are easy to enrich and difficult to eliminate, because inorganic pollutants cannot be decomposed naturally and can exist in other forms in the environment [1]. Among the toxic heavy metals, chromium is considered to be one of the most toxic metals due to its extensive utilization in the field of painting and leather. Chromium ions not only lead to significant environmental pollution but also result in irreversible harm to the human body [2]. Chromium usually exists in the form of Cr(VI) and Cr(III). However, Cr(VI) is generally more toxic than Cr(III), and even a very small amount of Cr(VI) can cause serious harm to the human body [3]. Therefore, to minimize the risks of contamination caused by excessive Cr(VI), it is urgent to reduce the concentration of Cr(VI) in industrial wastewater before discharge.

At present, various Cr(VI) wastewater treatment methods have been employed to eliminate Cr(VI) from wastewater, including chemical precipitation, reduction, ion exchange, membrane separation, and adsorption methods [4]. Among these approaches, adsorption has been widely considered for its advantages such as simplicity, efficiency, and environmental protection. Over the past few decades, a series of Cr(VI) adsorption

materials, including activated carbon, biomass, synthetic polymer resin, and clay minerals have been developed [5]. The biomass derived from low-cost agricultural and forestry wastes has gained significant attention in the field of wastewater treatment due to its environmental sustainability and cost-effectiveness [1,6].

Recently, bamboo char (BC) has attracted increasing research attention due to its stable physicochemical properties and large surface area, and it has been widely employed to remove hazardous contamination [7,8]. Its adsorption performance not only relies on the porous structure of the biochar, but also depends on the surface physical and chemical properties, such as cavity and heteroatom-containing functional groups [9–11]. To further improve the adsorption performance towards heavy metal ions and dyes of pure BC, surface modification based on doping and grafting is necessary [12–14].

To date, many BC-based biosorbents have been developed for wastewater treatment. For example, Ca-based magnetic BC was synthesized and used for Pb(II) ion removal, and a maximum adsorption capacity of 475.58 mg/g was obtained [15]. The proposed adsorption mechanism revealed that the usefulness of Ca-based magnetic bamboo-derived hydrochar for Pb(II) removal was due to electrostatic attraction, ion exchange, complexation, and reduction. Copper-modified BC was fabricated via the method of impregnation, and used for the removal of 15 toxic metals from industrial wastewater [16]. The obtained results showed that most ions in the mixture could reach equilibrium within 3 h, and a high removal efficiency was observed for Cd, Pb, As, and Cr. Ni doping BC was also reported by Wang and co-workers [17], and used for the adsorption of Pb(II). A much higher adsorption capacity of Pb(II) was observed for Ni-BC (142.7 mg/g) than that of pure BC (25 mg/g), which can be ascribed to the improved surface properties given by Ni-doping. To further improve the adsorption capacity of pure BC towards Cr(VI) [18], hydrothermal pyrolysis of bamboo sawdust was conducted with ZnCl₂ or AlCl₃. The pore volume and surface area were improved dramatically after being modified with ZnCl₂ and AlCl₃, and the highest adsorption capacity was increased by 3.4 and 2.8 times, respectively.

In addition, polyitaconate-functionalized BC was fabricated through free radical polymerization and used for Pb(II) adsorption [19]. The highest adsorption capacity for Pb(II) was 291.8 mg/g, and its adsorption behavior matched the pseudo-second-order kinetics equations. A cation-functionalized BC was fabricated for Cr(VI) removal by firstly grafting glyceride methacrylate (GMA) with the free radical initiator of benzoyl peroxide, followed by the amination of diethylenetriamine and protonation of hydrochloric acid [20]. A high adsorption capacity of 424.09 mg/g was obtained for Cr(VI), with an initial Cr(VI) concentration of 600 mg/g.

The modification of bamboo char can significantly improve the removal efficiency of toxic metal ions from wastewater. Electron beam irradiation technology has received increasing attention as an economical and environmentally sustainable alternative to traditional chemical treatment methods. This method is clean, solvent-free, time-saving, eco-friendly, and operationally efficient. However, there are few reports that focus on the radiation grafting modification of bamboo. Electron beam irradiation-induced grafting has many advantages over traditional chemical initiation grafting, including no need for initiators, a faster process, energy efficiency, environmental friendliness, safety, and wider applications [21–23]. Therefore, a novel cation-functionalized bamboo char (BC) is fabricated via the electron beam irradiation grafting method in this work. The BC is first grafted with glycidyl methacrylate (GMA) through electron beam irradiation, and then, chemically modified with diethylenetriamine (DGBC), and finally, protonated via treatment with hydrochloric acid to obtain diethyltriamine-functionalized BC (CDGBC). The modification of the BC can significantly improve its ability to remove Cr(VI) in wastewater. At the same time, the fabricated CDGBC is determined via FTIR, SEM, TG, XRD, and Zeta potential. The obtained CDGBC is used for the removal of Cr(VI) in various conditions, such as different initial concentrations, pH levels, and adsorption times. In addition, the adsorption kinetics, isothermal model, and adsorption thermodynamics are investigated, and the possible mechanism of Cr(VI) adsorption is also proposed. This work reveals that

the electron beam radiation grafting method is an efficient and environmentally friendly approach to BC modification, and can be used for the enhanced trapping of toxic metal ions in industrial wastewater.

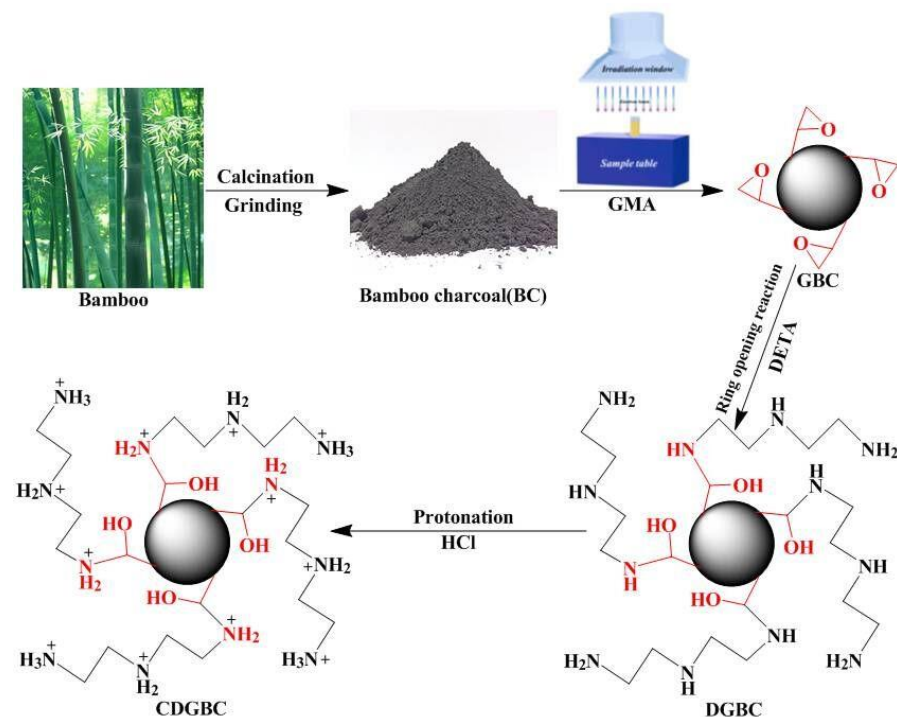
2. Materials and Methods

2.1. Materials and Chemicals

Bamboo char was purchased from a local reagent company (Xianning, China). Glycidyl methacrylate (GMA) and diphenylcarbazide were supplied by Aladdin Reagents (Shanghai, China). Potassium dichromate, diethylenetriamine (DETA), ethanol, sodium sulfate, hydrochloric acid, sodium hydroxide, and acetone were provided by Sinopharm Chemical Reagent Co., Ltd., Shanghai, China. The chemicals used were of analytical grade, and ultra-pure water (18.25 M Ω) was used throughout the study.

2.2. Preparation of CDGBC

The CDGBC was fabricated via electron beam irradiation grafting, which is schematically presented in Scheme 1. Firstly, alkali-activated BC was prepared through the following method [24]: A total of 10 g bamboo char was mixed with 5 wt% NaOH solution for activation under magnetic stirring for 1 h at 25 °C. The char was washed with distilled water several times until it reached a stable pH, and then, dried at 60 °C to a constant weight. Secondly, 1.0 g activated BC was packaged in a polyethylene bag, 50 mL 30% (v/v) GMA solution was added, and it was purged with nitrogen for 5 min. The sealed solid–liquid mixture was irradiated using an electron accelerator (1 MeV, Wasik Associates, USA) at room temperature, with a total adsorbed dose of 100 kGy and dose rate of 20 kGy/pass. After the grafting reaction, the obtained GBC sample was washed with methanol and deionized water to remove unreacted reagents, and then, dried at 50 °C for further use. Thirdly, 0.2 g of GBC was suspended in a solution of 0.6 g DETA/10 mL ethanol, and the mixture was reacted at 75 °C for 18 h. After filtration and washing with ethanol and water, the product was dried in an oven at 50 °C for 3 h. The resulting product was referred to as DGBC. Finally, the obtained DGBC was immersed in 50 mL 1 M HCl and stirred continuously for 3 h [25]. The obtained samples were washed with water and dried overnight, and were marked as CDGBC.



Scheme 1. The synthesis of CDGBC.

2.3. Characterization

FT-IR was measured via a NICOLET 5700 spectrometer (Thermo Fisher Nicolet, Waltham, MA, USA). The thermal stability of the sample was characterized using a TG 209 F3 thermogravimetric analyzer under a N₂ atmosphere, with a heating rate of 10 °C/min between ambient temperature and 700 °C (NETZSCH, Waldkraiburg, Germany). The morphology and microstructure were evaluated using a VEGA-3 SBH scanning electron microscope (Tescan, Brno, Czech Republic). Surface charges of DFBC were observed using a Zetasizer Nano ZS90 device (Malvern, UK). X-ray powder diffraction (XRD) was observed using a LabX XRD6100 (Shimadzu, Kyoto, Japan). The samples were irradiated using an electron accelerator (1 MeV, Wasik Associates, Dracut, MA, USA)

2.4. Batch Adsorption of Cr(VI)

The adsorption performance of CDGBC was evaluated via batch experiments in duplicate. At each run, 20 mg of the prepared CDGBC was added to 20 mL of solution in a 50 mL transparent glass bottle, and then, agitated on a thermostatic oscillator shaken at a rate of 180 rpm at a certain temperature; for the kinetics study, the temperature was 298.15 K, and for the isothermal study, the temperatures were 298.15 K, 308.15 K, and 318.15 K.

The pH value of the Cr(VI) solution was adjusted by 0.1 M NaOH or 0.1 M HCl, when exploring the effect of pH value on the adsorption performance of CDGBC, with an initial Cr(VI) concentration of 300 mg/L at 298.15 K.

After each Cr(VI) adsorption experiment, a 0.45 µm polypropylene syringe filter was used for membrane separation to collect filtrate. The Cr(VI) concentration was tested with diphenylcarbazide using a UV-vis spectrophotometer (UV1901), at a wavelength of 540 nm. For the adsorption kinetic experiment, the residual chromium solution was collected at variable time intervals within 480 min. For the adsorption isotherm test, residual Cr(VI) solution with different initial concentrations was collected at equilibrium time at different temperatures.

The capacity of adsorption (Q , mg/g), and removal efficiency (R , %) were calculated using Equations (1)–(3) [23,25]:

$$Q = \frac{(C_0 - C_e)V}{m} \quad (1)$$

$$R = \frac{C_0 - C_e}{C_0} \times 100\% \quad (2)$$

$$Q = \frac{(C_0 - C_t)V}{m} \quad (3)$$

where C_0 (mg/L) is the initial concentration of Cr(VI); C_e (mg/L) is the equilibrium concentration of Cr(VI); C_t (mg/L) is the concentration of Cr(VI) at time t ; V (mL) is the volume of the solution; and m (g) is the mass of the CDGBC.

3. Results and Discussion

3.1. Structure Analysis

The FTIR spectra of the obtained BC, GBC, DGBC, and CDGBC in Figure 1 demonstrate the successful grafting of GMA, amination, and the protonation of BC. For the spectra of pure BC (Figure 1a), characteristic peaks at 3685 cm⁻¹ (O-H stretching), 2982 cm⁻¹ (-CH₃ stretching), 2354 cm⁻¹ (accumulate C=C stretching or C≡C), and 1079 cm⁻¹ (C-O deformation vibration) are observed [26]. New peaks at 850, 908, and 1160 cm⁻¹ attributed to epoxide groups at 1721 cm⁻¹ (C=O stretching) are observed in Figure 1b, indicating that GMA was successfully grafted to the BC [22]. For the spectra of DGBC (Figure 1c), the characteristic peaks for the epoxide groups almost disappear, which can be ascribed to the reaction with DETA. In addition, new peaks at 1064 cm⁻¹ (C-N stretching vibration), and 3745 cm⁻¹ (N-H stretching vibration) appear, indicating that DETA was successfully reacted with GBC [22,23]. After the protonation of amine (Figure 1d), the peak intensity of the

nitrogen-containing group decreases obviously, indicating the protonation of amine [20,25].

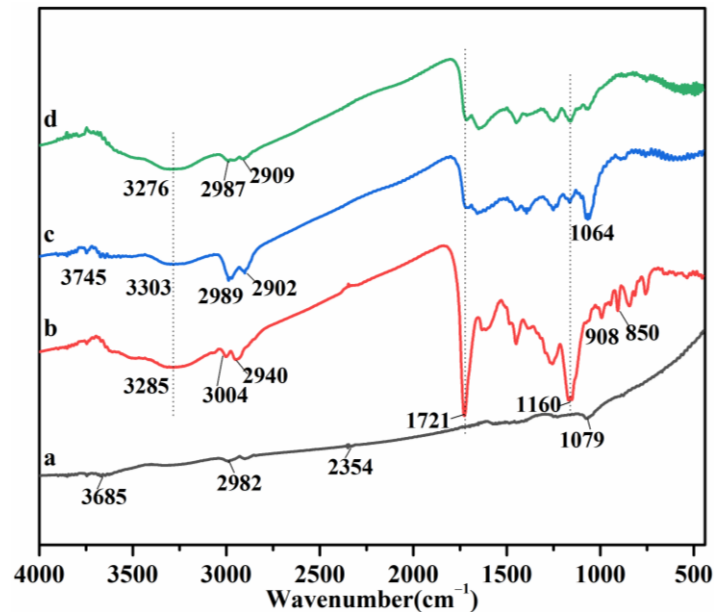


Figure 1. FTIR spectra of (a) BC; (b) GBC; (c) DGBC; (d) CDGBC.

3.2. Morphology Analysis

The morphology of pure BC and the product at different stages are shown in Figure 2. Pure BC exhibits rough surfaces and macroporous structures, which originated from the materials [27,28]. With the grafting of GMA, the macroporous structure was not completely plugged, which will be more favorable for the Cr(VI) adsorption process [20,25]. No obvious morphology change was observed for DGBC and CDGBC, which is consistent with the reported work in [21,22]. The rougher surface and reserved macroporous structure of CDGBC, as well as the loaded functional groups, could enhance its pollutant removal performance.

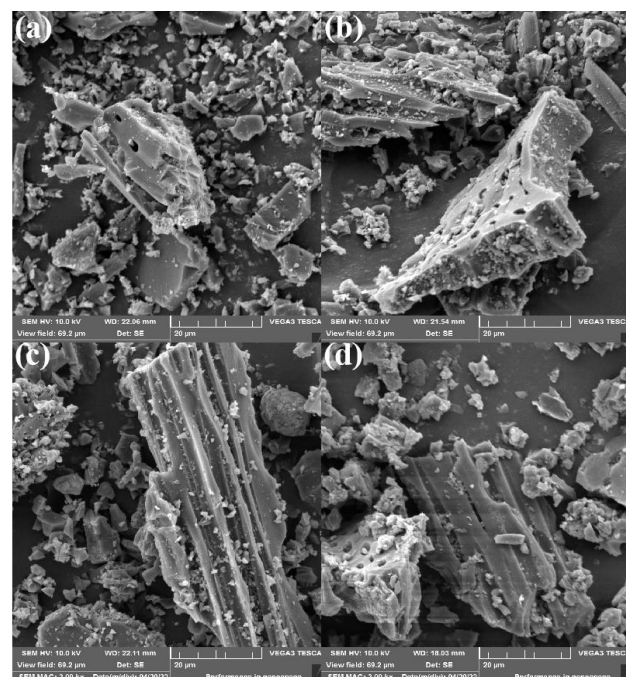


Figure 2. SEM images of (a) pure BC; (b) GBC; (c) DGBC; (d) CDGBC.

3.3. TGA Analysis

In order to explore the composition and thermal stability of the BC, GBC, DGBC, and CDGBC, TG analysis was conducted (Figure 3). As represented in Figure 3a, the pure BC showed the greatest thermal stability, with only 1.7% weight loss observed before 100 °C, which can be ascribed to the release of adsorbed water. During this stage, the highest mass loss rate appeared at 58.5 °C. Before the temperature of 700 °C, only 8.2 wt% weight loss was found for the pure BC, which was due to the volatilization of water and volatile compounds [29]. At this stage, the highest mass loss rate appeared at 371.6 °C, 503.8 °C, and 619.3 °C. The thermal degradation of GBC is shown in Figure 3b. The decomposition of GBC was divided into three stages, namely, before 210 °C, 210–420 °C, and after 420 °C. The GBC and BC showed no significant differences in the first and third stages. The weight loss of GBC at the second stage is mainly ascribed to the decomposition of grafted GMA; thus, the grafting yield of GMA was calculated to be 3.5 wt% [22,23]. Additionally, the highest mass loss rate during this stage took place at 128.9 °C, higher than the counterpart for BC, indicating that thermostability increased after the irradiation grafting method.

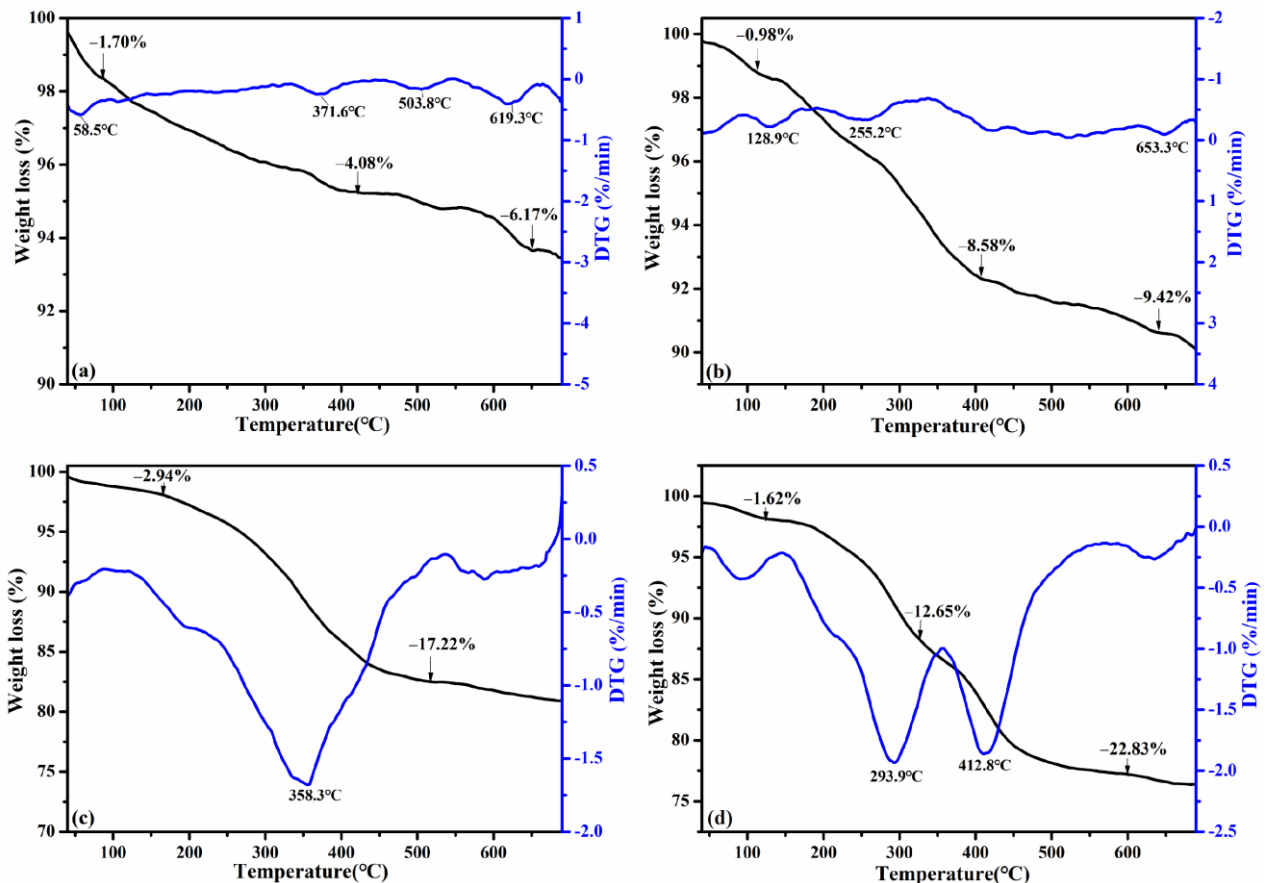


Figure 3. TG and DTG curves of (a) BC; (b) GBC; (c) DGBC; (d) CDGBC.

The decomposition of DGBC and CDGBC was more complete than that of GBC; the considerable weight loss not only reveals the low thermal stability of DGBC and CDGBC, but also demonstrates successful amination and protonation. Sharp weight loss is observed between 210 and 480 °C in Figure 3c, which is mainly attributed to the grafted GMA and DETA, with a percentage of 12.8%. According to the grafting yield of GMA, the weight ratio of reacted DETA was calculated to be 9.3%. The decomposition of DGBC was similar to that of CDGBC, while more weight loss (15.4%) was observed between 210 to 480 °C for CDGBC (Figure 3d). In this segment, the highest weight loss was revealed at 293.9 °C and 412.8 °C, which may be ascribed to the salinization of amine and hydrochloric acid [20,25].

3.4. XRD Analysis

The XRD patterns for pure BC, CDGBC, and after contact with Cr(VI) are presented in Figure 4. Each sample exhibits wide peaks, which represent the features of amorphous substances [30]. Peaks are observed at approximately 24° and 43°. The wide diffraction peak of the adsorbent at approximately 24° belongs to the (002) of graphite carbon.

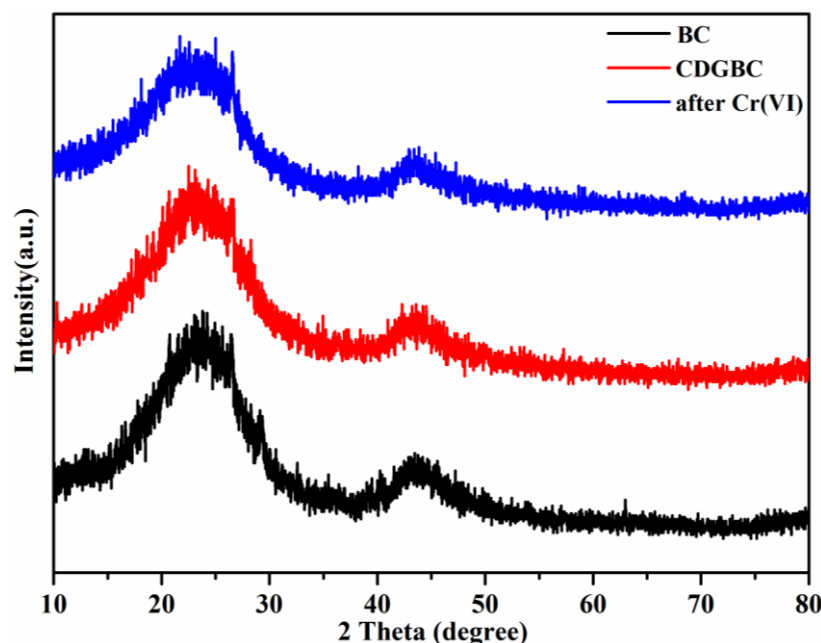


Figure 4. XRD of pure BC, CDGBC, and CDGBC after contact with Cr(VI).

For CDGBC and CDGBC after contact with Cr(VI), the diffraction peaks of BC overlap with others, while the intensity is slightly weakened. The results indicate that the crystal structure of the CDGBC did not change after Cr(VI) adsorption. Generally speaking, the disordered arrangement of amorphous materials is considered to be positive for the adsorption process [31].

3.5. Adsorption Behavior of CDGBC

3.5.1. Effect of pH

The initial pH of the solution is very important to the uptake process. It not only determines the surface charge form of the adsorbent, but also affects the existing form of chromium in the solution. So, the study of optimal pH is very important for Cr(VI) adsorption [32,33]. The effect of the pH value on the uptake of Cr(VI) was studied in the range of 2.0 to 10.0 at 298.15 K. As shown in Figure 5a, the adsorption of Cr(VI) was highly dependent on the solution pH value, the adsorption capacity of Cr(VI) decreased obviously with the increase in the solution pH value, demonstrating that the solution pH has an important influence on the Cr(VI) adsorption capacity. As reported in the literature [34,35], the Cr ion exists as $\text{Cr}_2\text{O}_7^{2-}$ and HCrO_4^- at pH ranged within 2.0~6.0, and transforms to CrO_4^{2-} when $\text{pH} > 6.0$. On the other hand, as shown in Figure 5b, the zeta potential of BC varied from 4.29 to -39.12 mV when the pH increased from 2.0 to 10.0, and the point of no charge appeared at $\text{pH} = 2.5$. CDGBC varied from 41.90 to -22.76 mV between pH 2.0 and 10.0, and the point of no charge increased to $\text{pH} = 7.3$. Compared to pure BC, a more positive charge was observed for the CDGBC, which is a benefit for the adsorption of the negative $\text{Cr}_2\text{O}_7^{2-}$, HCrO_4^- , and CrO_4^{2-} . The protonation degree decreased with the increase in the solution pH value, leading to a decrease in the electrostatic interaction between CDGBC and Cr(VI) ions; this is the reason why the adsorption capacity of Cr(VI) decreased with an increase in solution pH value [20,25].

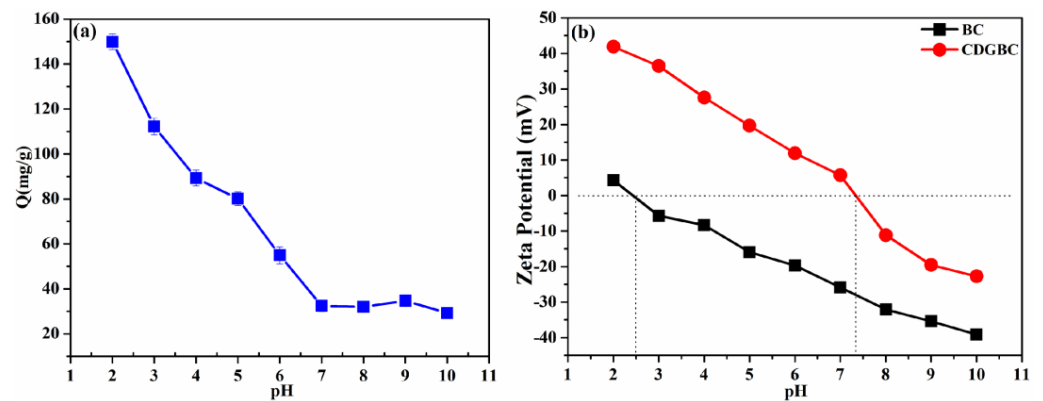


Figure 5. Effect of pH value on Cr(VI) adsorption of CDGBC (a), and Zeta potential of pure BC and CDGBC (b) (adsorbed dose = 100 kGy, $C_0 = 300$ mg/L, contact time = 24 h).

3.5.2. Adsorption Kinetics

The influence of adsorption time was studied with a Cr(VI) concentration of 200 mg/L and pH = 2. As revealed in Figure 6, at the initial stage, the adsorption capacity increases gradually with the extension of contact time and the equilibrium of adsorption is reached at 360 min.

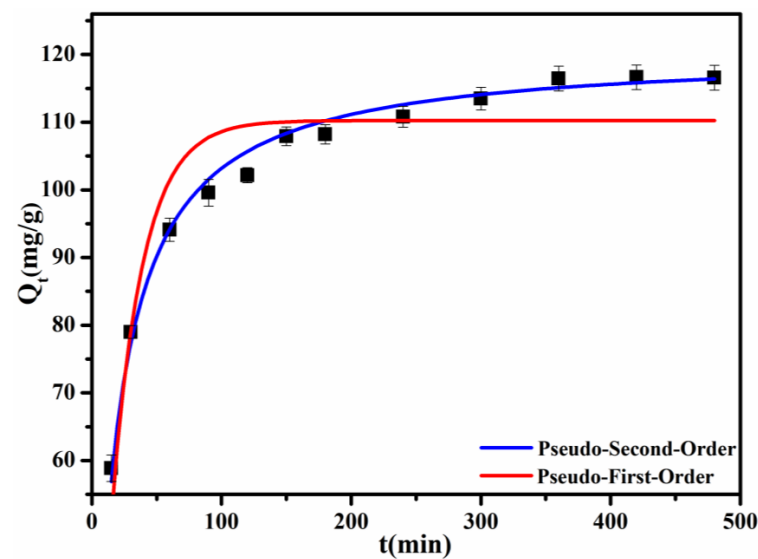


Figure 6. Effect of adsorption time of Cr(VI) on Q_t ; fitting plots of pseudo-second-order and pseudo-first-order models (pH = 2, $C_0 = 200$ mg/L, $T = 298.15$ K).

In this study, adsorption kinetics models were applied to predict the rate-limiting steps in the Cr(VI) uptake process. Two kinetic adsorption models, including pseudo-first-order [36] and pseudo-second-order [37] models, were used to fit the adsorption process (Figure 5b,c). The two models were calculated using Equations (4) and (5):

$$\frac{dQ_t}{dt} = k_1(Q_e - Q_t) \quad (4)$$

$$\frac{dQ_t}{dt} = k_2(Q_e - Q_t)^2 \quad (5)$$

where Q_t and Q_e (mg/g) stand for Cr(VI) adsorption capacity at time t and equilibrium, separately; k_1 (min^{-1}) and k_2 ($\text{g} \cdot \text{mg}^{-1} \cdot \text{min}^{-1}$) represent the rate constant with different models, separately.

As shown in Table 1, the coefficient (R^2) of the pseudo-second-order model is 0.9901, which is higher than that of the pseudo-first-order model ($R^2 = 0.8807$). In addition, $Q_{e,cal}$ obtained with the pseudo-second-order model was closer to the experimental value than that of the pseudo-first-order model. These results demonstrate the validity of the pseudo-second-order model for predicting the Cr(VI) adsorption process. Based on the aforementioned findings, the adsorption of Cr(VI) onto CDGBC was mainly a chemisorption-controlled process [38,39].

Table 1. Kinetic parameters of Cr(VI) adsorbed onto CDGBC at 298.15 K.

Adsorption Kinetics Models	Coefficients	Cr (VI)
Pseudo-first-order	Q_e, exp (mg/g)	118.63
	Q_e, cal (mg/g)	110.25
	k_1 (L/g)	0.04203
	R^2	0.8807
Pseudo-second-order	Q_e, cal (mg/g)	120.45
	k_2 (g/mg·min)	4.954×10^{-4}
	R^2	0.9901

3.5.3. Adsorption Isotherm

Adsorption isotherms are widely used to describe the relationship between adsorption capacity and equilibrium concentration [5]. To investigate the relationship of the uptake capacity with different initial Cr(VI) concentrations, adsorption isotherms were conducted with diverse initial concentrations from 100 to 400 mg/L at different temperatures. The initial Cr(VI) concentration vs. adsorption capacity, and equilibrium concentration vs. adsorption capacity, are plotted in Figure 7a. The adsorption capacity of Cr(VI) ions increased rapidly, and then, slowly with the increase in initial concentration. In addition, the Cr(VI) adsorption capacity also increased with the temperature increase [40], and the maximum adsorption capacity of CDGBC calculated from Figure 6a was 169.13 mg/g. Two isotherm models, namely, Langmuir and Freundlich, were utilized to plot the adsorption at 298.15 K, 308.15 K, and 318.15 K (Figure 7b), respectively. The isotherm parameters can be calculated using Equations (6) and (7):

$$Q_e = \frac{Q_m K_L C_e}{1 + K_L C_e} \quad (6)$$

$$Q_e = K_F C_e^{1/n} \quad (7)$$

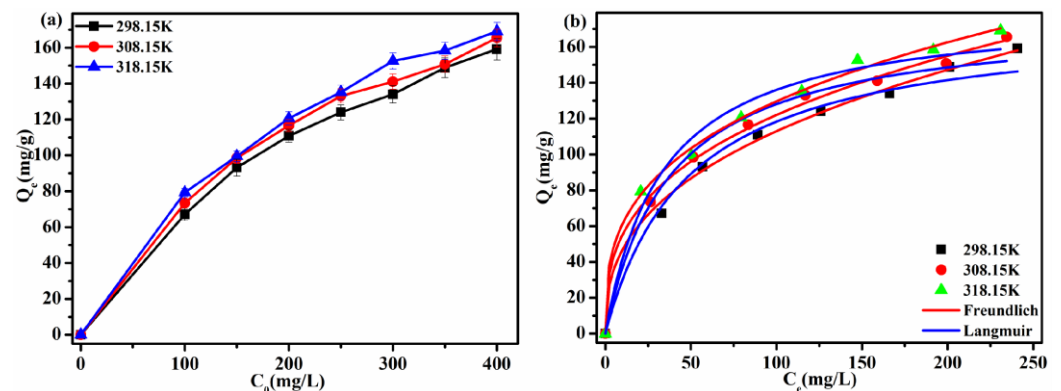


Figure 7. (a) The effect of initial Cr(VI) concentration; (b) the isotherm, Langmuir, and Freundlich curves (contact time = 24 h, pH = 2, T = 298.15 K, 308.15 K, 318.15 K).

In the equations, Q_e (mg/g) represents the adsorption capacity at equilibrium; C_e (mg/L) represents the Cr(VI) concentrations at equilibrium; Q_m (mg/g) is the maxi-

mal adsorption capacity; K_L (L/mg) is the constant of Langmuir; K_F ($\text{mg}^{1-1/n} \cdot \text{L}^{1/n} \cdot \text{g}^{-1}$) denotes the Freundlich constant; and $1/n$ represent the heterogeneity factor.

The results of fitting the two isotherm models are shown in Table 2; the Freundlich model showed a higher linear correlation ($R^2 = 0.9962$ – 0.9969) compared with Langmuir ($R^2 = 0.9806$ – 0.9888). Thus, the Cr(VI) adsorption process was obeyed by the Freundlich isotherm model, indicating that multilayer adsorption is the main process in the removal of Cr(VI) by CDGBC.

Table 2. Isothermal parameters of Cr(VI) adsorbed onto CDGBC.

Isothermal Model	Parameters	Different Temperatures (K)		
		298.15	308.15	318.15
Langmuir	Q_m (mg/g)	175.87	176.75	181.79
	K_L (L/mg)	0.0206	0.0263	0.0297
	R^2	0.9863	0.9888	0.9806
Freundlich	K_F ($\text{mg}^{1-1/n} \cdot \text{L}^{1/n} \cdot \text{g}^{-1}$)	19.395	24.844	28.795
	n	2.6138	2.8939	3.0613
	R^2	0.9962	0.9964	0.9969

3.5.4. Adsorption Thermodynamics

Thermodynamic analysis was used to evaluate the thermal effect and spontaneous nature of the adsorption process. To calculate the thermodynamic factors, Gibbs free energy change ΔG , enthalpy change ΔH , and entropy change ΔS were required. All of the thermodynamic parameters were calculated at 298.15 K, 308.15 K, and 318.15 K according to Equations (8) and (9) [38,41]:

$$\ln\left(\frac{Q_e}{C_e}\right) = -\frac{\Delta H}{R} \times \frac{1}{T} + \frac{\Delta S}{R} \quad (8)$$

$$\Delta G = \Delta H - T\Delta S \quad (9)$$

Table 3 shows the thermodynamic parameters calculated from the equations. The negative ΔG reveals the spontaneous and thermodynamically favorable process of Cr(VI) adsorbed onto CDGBC. The ΔG values at 298.15 K, 308.15 K, and 318.15 K were -0.54 , -0.86 , and -1.11 kJ/mol, respectively, indicating that the increase in temperature benefits the spontaneous progress [20].

Table 3. Thermodynamic data of Cr(VI) adsorbed onto CDGBC.

Concentration (mg/L)	T (K)	$\ln(Q_e/C_e)$	Thermodynamic Parameter			
			ΔH (kJ·mol ⁻¹)	ΔS (J·mol ⁻¹ ·K ⁻¹)	ΔG (kJ·mol ⁻¹)	R^2
200	298.15	0.2183	7.90	28.35	-0.54	0.9894
	308.15	0.3343			-0.86	
	318.15	0.4184			-1.11	

The positive value of ΔS suggests that the adsorption process was random at the interface of CDGBC. Furthermore, the adsorption process of Cr(VI) on CDGBC could increase the entire system's freedom degree. In addition, the positive value of ΔH indicates that the endothermic adsorption process, which occurs only at high temperatures, can be achieved, which is attributed to the increased active sites at high temperatures. In addition, the ΔH was 7.90 kJ/mol, indicating that the Cr(VI) was mainly adsorbed onto CDGBC through chemisorption; this result is consistent with the kinetic data [40].

3.6. Possible Mechanism of Cr(VI) Uptake on CDGBC

The changes in functional groups before and after CDGBC's adsorption of Cr(VI) play an important role in the understanding of the adsorption mechanism. The FTIR spectra of CDGBC and CDGBC after the uptake of Cr(VI) are presented in Figure 8. The broad adsorption peaks at 2987 and 3276 cm^{-1} are ascribed to the stretching vibration of C-H and N-H/O-H, respectively. After Cr(VI) adsorption, the peaks slightly shift to 2918 and 3416 cm^{-1} . While the peaks at 2900–3000 cm^{-1} are weakened evidently; it is proven that the amine and hydroxyl groups participated in Cr(VI) uptake. Obviously, new bands appeared at 915 and 693 cm^{-1} , which could be ascribed to Cr=O and Cr-O stretching vibrations, respectively [20]. The migration of some characteristic peaks and the appearance of new characteristic peaks confirm that Cr(VI) was successfully uptaken by CDGBC.

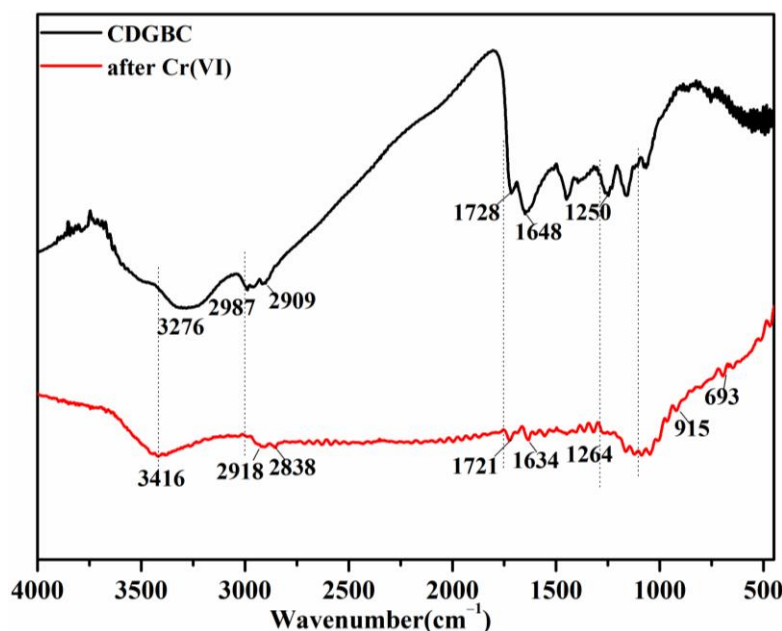
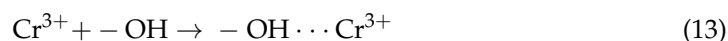
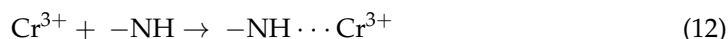
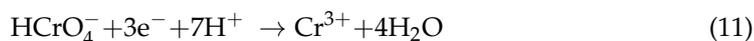


Figure 8. FTIR spectra of CDGBC and CDGBC after Cr(VI).

According to the above obtained results, possible adsorption mechanisms of Cr(VI) adsorbed on CDGBC are proposed. Based on the adsorption performance at a pH range of 2–10 and the surface zeta potential analysis of CDGBC, it is proven that electrostatic interaction plays an important role in the process of Cr(VI) adsorption. This is because the cationic groups of $-\text{NH}_2\text{R}^+$ ($-\text{NH}_2^+$ or $-\text{NH}_3^+$) on the CDGBC could capture Cr(VI) through an electrostatic interaction under strong acidic conditions [20], as shown in the following equation:



In addition, the groups of $-\text{NH}_3^+$, $-\text{NH}_2^+$, and $-\text{OH}$ could donate electrons to convert a part of the adsorbed Cr(VI) to Cr(III) [42]. Due to the repulsion of the electrostatic charge between CDGBC and Cr(III), the cationic Cr(III) escapes from CDGBC to the solution and can be fixed onto the surface of CDGBC through complexation with $-\text{NH}$ and $-\text{OH}$, as shown in the following equations:



Therefore, besides the electrostatic interaction, pore adsorption and complexation were also involved in the Cr(VI) capture of CDGBC, which is consistent with the experiment result and previous studies [20,40].

3.7. The Effect of Ions Competing for Cr (VI) Uptake

The impact of coexisting ions on the uptake of Cr(VI) by CDGBC was investigated and is displayed in Figure 9. SO_4^{2-} solutions with different concentrations were studied. The uptake capacity of CDGBC decreased dramatically from 110.87 to 37.62 mg/g as the concentration of SO_4^{2-} increased from 0 to 2.0 mol/L (Figure 9). Obviously, with the addition of sulfate, it has a strong effect on chromium adsorption, which is due to the competitive electrostatic attraction between sulfate and $\text{Cr}_2\text{O}_7^{2-}$.

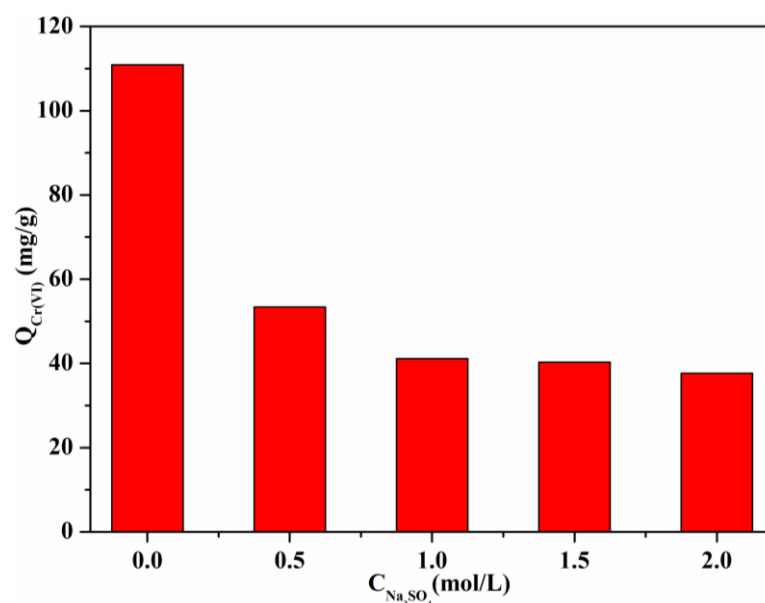


Figure 9. Effect of competing ion concentrations on adsorption capacities of Cr(VI) by CDGBC ($C_0 = 200$ mg/L, CDGBC dosage = 20 mg; pH = 2, t = 24 h, T = 298 K).

3.8. Comparison of Intermediate Product with CGDBC for Cr (VI) Removal

The adsorption capacities of BC, GBC, DGBC and CDGBC are displayed in Table 4. As observed in the results, the uptake capacities of BC and GBC towards Cr(VI) were only 16.24 and 12.17 mg/g, respectively. However, after amination with DETA, the adsorption capacity of Cr(VI) increased. However, the adsorption capacity of CDGBC on Cr(VI) was significantly improved after protonation.

Table 4. Adsorption capacity of Cr(VI) for different adsorbents (t = 24 h, $C_0 = 200$ mg/L).

Samples	Adsorption Capacity (mg/g)
BC	16.24
GBC	12.17
DGBC	74.53
CDGBC	110.87

3.9. Comparison of CGDBC with Other Adsorbents for Cr (VI)

Table 5 compares the Cr(VI) removal parameters of CDGBC with other bamboo-based adsorbents, including their maximal adsorption capacity (Q_{max}), experimental conditions, and equilibrium time. According to the experimental results, CDGBC exhibited a good adsorption capacity compared with other low-cost bamboo-based adsorbents, which reveals that CDGBC is an excellent adsorbent. It also provides a new method for Cr(VI) removal from contaminated water.

Table 5. Comparison of CDGBC and other bamboo-char-based adsorbents towards Cr(VI).

Adsorbent	Experimental Conditions (pH, T/°C)	Q _{max} (mg/g)	Adsorption Equilibrium Time (min)	Ref.
CDGBC	pH = 2, Temp. = 45 °C	169.13	360	This work
Chitosan-modified magnetic bamboo biochar (CMBB)	pH = 2, Temp. = 25 °C	127	300	[43]
Magnetic bamboo biochar (MBB)	pH = 1, Temp. = 25 °C	75.8	500	[43]
Nitrilotriacetic acid-modified bamboo charcoal (NTA-MBC)	pH = 3, Temp. = 25 °C	270	60	[44]
Iron-modified bamboo charcoal	pH = 5, Temp. = 15 °C	35.7	480	[44]
Cobalt and iron binary oxide bamboo charcoal	pH = 5, Temp. = 15 °C	51.7	480	[45]
Iron-loaded carbon aerogels derived from bamboo	pH = 2, Temp. = 25 °C	182	8	[46]

4. Conclusions

In summary, cation-functionalized bio-based CDGBC with excellent Cr(VI) adsorption capacity was successfully fabricated through the electron beam radiation grafting method. The FT-IR results demonstrate the successful preparation of CDGBC biosorbent, while the SEM results indicate its reserved rough surface and macroporous structure. The XRD results reveal the amorphous structure of the adsorbent, and the TG results show a grafting yield of 3.5 wt% for GMA. The results of the pH effect and zeta potential validate that electrostatic attraction contributes to the adsorption of Cr(VI) onto CDGBC. The kinetic results confirm that the adsorption process obeys the pseudo-second-order kinetic model, indicating that chemisorption is the main adsorption process. The isotherm results display that the highest adsorption capacity of CDGBC is 169.13 mg/g, and the process of Cr(VI) adsorption is a multi-layered process. This study provides valuable insights into the design of a highly efficient biosorbent derived from bamboo char, specifically tailored for the uptake of heavy metals. These advancements will greatly enhance the industrial application potential of BC-based biosorbents.

Author Contributions: Conceptualization, Y.Z. and T.C.; investigation, J.G. and X.H.; structure characterization, J.G., T.L. and X.H.; data analysis, B.L. and G.H.; writing—original draft, Y.Z. and T.C.; writing—review and editing, B.L. and T.L.; supervision and administration, G.H. All authors have read and agreed to the published version of the manuscript.

Funding: This work was supported by grants from the National Natural Science Foundation of China (12175200, 51903080), the Foundation of Hubei Provincial Department of Education (D20212801, B2021223), and the Scientific Research Foundation of Hubei University of Science and Technology (2022T03, 2022ZX10, 2022ZX12, 2022ZX13, H2019006).

Institutional Review Board Statement: Not applicable.

Informed Consent Statement: Not applicable.

Data Availability Statement: Not applicable.

Conflicts of Interest: The authors declare no conflict of interest.

References

- Sahu, U.K.; Zhang, Y.; Huang, W.; Ma, H.; Mandal, S.; Sahu, S.; Sahu, M.K.; Patel, R.K.; Pu, S. Nanoceria-loaded tea waste as bio-sorbent for Cr(VI) removal. *Mater. Chem. Phys.* **2022**, *290*, 126563. [[CrossRef](#)]
- Su, Q.; Khan, A.A.; Su, Z.; Tian, C.; Li, X.; Gu, J.; Zhang, T.; Ahmad, R.; Su, X.; Lin, Z. Novel nitrogen-doped KFeS₂/C composites for the efficient removal of Cr(VI). *Environ. Sci. Nano.* **2021**, *8*, 1057–1066. [[CrossRef](#)]
- Kong, A.; Sun, Y.; Peng, M.; Gu, H.; Fu, Y.; Zhang, J.; Li, W. Amino-functionalized MXenes for efficient removal of Cr(VI). *Colloid Surface A* **2021**, *617*, 126388. [[CrossRef](#)]

4. Yang, J.; Song, Y.; Yue, Y.; Liu, W.; Che, Q.; Chen, H.; Ma, H. Chemically dual-modified biochar for the effective removal of Cr(VI) in solution. *Polymers* **2022**, *14*, 39. [[CrossRef](#)]
5. Orooji, Y.; Nezafat, Z.; Nasrollahzadeh, M.; Kamali, T.A. Polysaccharide-based (nano) materials for Cr(VI) removal. *Int. J. Biol. Macromol.* **2021**, *188*, 950–973. [[CrossRef](#)] [[PubMed](#)]
6. Bai, S.Z.; Wang, T.T.; Tian, Z.S.; Cao, K.S.; Li, J.T. Facile preparation of porous biomass charcoal from peanut shell as adsorbent. *Sci. Rep.* **2020**, *10*, 15845. [[CrossRef](#)] [[PubMed](#)]
7. Mui, E.L.K.; Cheung, W.H.; Valix, M.; McKay, G. Dye adsorption onto char from bamboo. *J. Hazard. Mater.* **2010**, *177*, 1001–1005. [[CrossRef](#)]
8. Liao, P.; Ismael, Z.M.; Zhang, W.B.; Yuan, S.H.; Tong, M.; Wang, K.; Bao, J.G. Adsorption of dyes from aqueous solutions by microwave modified bamboo charcoal. *Chem. Eng. J.* **2012**, *195*, 339–346. [[CrossRef](#)]
9. Li, H.; Gao, P.; Cui, J.; Zhang, F.; Wang, F.; Cheng, J. Preparation and Cr(VI) removal performance of corncob activated carbon. *Environ. Sci. Pollut. Res.* **2018**, *25*, 20743–20755. [[CrossRef](#)]
10. Cao, W.; Wang, Z.; Ao, H.; Yuan, B. Removal of Cr(VI) by corn stalk based anion exchanger: The extent and rate of Cr(VI) reduction as side reaction. *Colloid Surface A* **2018**, *539*, 424–432. [[CrossRef](#)]
11. Nadarajah, K.; Bandala, E.R.; Zhuang, X.; Mundree, S.; Goonetilleke, A. Removal of heavy metals from water using engineered hydrochar: Kinetics and mechanistic approach. *J. Water. Process. Eng.* **2021**, *40*, 101929. [[CrossRef](#)]
12. Chen, Q. Study on the adsorption of lanthanum(III) from aqueous solution by bamboo charcoal. *J. Rare Earth.* **2010**, *28*, 125–131. [[CrossRef](#)]
13. Wang, S.Y.; Tsai, M.H.; Lo, S.F.; Tsai, M.J. Effects of manufacturing conditions on the adsorption capacity of heavy metal ions by Makino bamboo charcoal. *Bioresour. Technol.* **2008**, *99*, 7027–7033. [[CrossRef](#)]
14. Li, Y.; Meas, A.; Shan, S.; Yang, R.; Gai, X. Production and optimization of bamboo hydrochars for adsorption of Congo red and 2-naphthol. *Bioresour. Technol.* **2016**, *207*, 379–386. [[CrossRef](#)] [[PubMed](#)]
15. Qu, J.; Lin, X.; Liu, Z.; Liu, Y.; Wang, Z.; Liu, S.; Meng, Q.; Tao, Y.; Hu, Q.; Zhang, Y. One-pot synthesis of Ca-based magnetic hydrochar derived from consecutive hydrothermal and pyrolysis processing of bamboo for high-performance scavenging of Pb(II) and tetracycline from water. *Bioresour. Technol.* **2022**, *343*, 126046. [[CrossRef](#)]
16. Thotagamuge, R.; Kooch, M.R.R.; Mahadi, A.H.; Lim, C.M.; Abu, M.; Jan, A.; Hanipah, A.H.A.; Khiong, Y.Y.; Shofry, A. Copper modified activated bamboo charcoal to enhance adsorption of heavy metals from industrial wastewater. *Environ. Nanotechnol. Monitor. Manag.* **2021**, *16*, 100562. [[CrossRef](#)]
17. Wang, Y.; Wang, X.; Wang, X.J.; Liu, M.; Wu, Z.; Yang, L.Z.; Xia, S.Q.; Zhao, J.F. Adsorption of Pb(II) from aqueous solution to Ni-doped bamboo charcoal. *J. Ind. Eng. Chem.* **2013**, *19*, 353–359. [[CrossRef](#)]
18. Li, F.; Zimmerman, A.R.; Hu, X.; Gao, B. Removal of aqueous Cr(VI) by Zn- and Al-modified hydrochar. *Chemosphere* **2020**, *260*, 127610. [[CrossRef](#)] [[PubMed](#)]
19. Teng, H.J.; Xia, T.; Li, C.; Guo, J.Z.; Chen, L.; Wu, C.Z.; Li, B. Facile solvent-free radical polymerization to prepare itaconate-functionalized hydrochar for efficient sorption of methylene blue and Pb(II). *Bioresour. Technol.* **2023**, *377*, 128943. [[CrossRef](#)] [[PubMed](#)]
20. Zhang, Y.; Guo, J.; Wu, C.; Huan, W.; Li, B. Enhanced removal of Cr(VI) by cation functionalized bamboo hydrochar. *Bioresour. Technol.* **2022**, *347*, 126703. [[CrossRef](#)]
21. Du, J.F.; Wu, Y.Z.; Dong, Z.; Zhang, M.M.; Yang, X.; Xiong, H.H.; Zhao, L. Single and competitive adsorption between Indigo Carmine and Methyl orange dyes on quaternized kapok fiber adsorbent prepared by radiation technique. *Sep. Purif. Technol.* **2022**, *292*, 121103. [[CrossRef](#)]
22. Chen, T.; Sun, N.; Zhao, Y.; Gao, J.; Hu, G.; Han, X.; Tian, Y.; Chen, L.; Huang, G.; Li, B. Removal of La(III) by amino-phosphonic acid functionalized polystyrene microspheres prepared via electron beam irradiation. *J. Saudi. Chem. Soc.* **2022**, *26*, 101564. [[CrossRef](#)]
23. Zhao, Y.; Liang, T.; Miao, P.; Chen, T.; Han, X.; Hu, G.; Gao, J. Green preparation of aminated magnetic PMMA microspheres via EB irradiation and its highly efficient uptake of Ce(III). *Materials* **2022**, *15*, 6553. [[CrossRef](#)]
24. Correa, C.R.; Ngamying, C.; Klank, D.; Kruse, A. Investigation of the textural and adsorption properties of activated carbon from HTC and pyrolysis carbonizates. *Biomass Conv. Bioref.* **2018**, *8*, 317–328. [[CrossRef](#)]
25. Kim, Y.J.; Park, J.; Bangm, J.; Kim, J.; Jin, H.J.; Kwak, H.W. Highly efficient Cr(VI) remediation by cationic functionalized nanocellulose beads. *J. Hazard. Mater.* **2022**, *426*, 128078. [[CrossRef](#)] [[PubMed](#)]
26. Fu, D.; Zhang, Y.H.; Lv, F.Z.; Chu, P.K.; Shang, J.W. Removal of organic materials from TNT red water by Bamboo Charcoal adsorption. *Chem. Eng. J.* **2012**, *193*, 39–49. [[CrossRef](#)]
27. Li, F.Y.; Zimmerman, A.R.; Hu, X.; Yu, Z.B.; Huang, J.; Gao, B. One-pot synthesis and characterization of engineered hydrochar by hydrothermal carbonization of biomass with ZnCl₂. *Chemosphere* **2020**, *254*, 126866. [[CrossRef](#)] [[PubMed](#)]
28. Zhang, S.; Sheng, K.C.; Yan, W.; Liu, J.L.; Shuang, E.; Yang, M.; Zhang, X.M. Bamboo derived hydrochar microspheres fabricated by acid-assisted hydrothermal carbonization. *Chemosphere* **2021**, *263*, 128093. [[CrossRef](#)] [[PubMed](#)]
29. Dai, L.L.; He, C.; Wang, Y.P.; Liu, Y.H.; Yu, Z.T.; Zhou, Y.; Fan, L.L.; Duan, D.L.; Ruan, R. Comparative study on microwave and conventional hydrothermal pretreatment of bamboo sawdust: Hydrochar properties and its pyrolysis behaviors. *Energy Convers. Manag.* **2017**, *146*, 1–7. [[CrossRef](#)]

30. Li, A.; Ge, W.; Liu, L.; Zhang, Y.; Qiu, G. Synthesis and application of amine-functionalized MgFe₂O₄-biochar for the adsorption and immobilization of Cd(II) and Pb(II). *Chem. Eng. J.* **2022**, *439*, 135785. [[CrossRef](#)]
31. Schio, R.D.R.; Martinello, B.D.K.; Netto, M.S.; Silva, L.L.O.; Mallmann, E.S.; Dotto, G.L. Adsorption performance of Food Red 17 dye using an eco-friendly material based on *Luffa cylindrica* and chitosan. *J. Mol. Liq.* **2021**, *349*, 118144. [[CrossRef](#)]
32. Hou, T.; Kong, L.; Guo, X.; Wu, Y.; Wang, F.; Wen, Y.; Yang, H. Magnetic ferrous-doped graphene for improving Cr(VI) removal. *Mater. Res. Express* **2016**, *3*, 045006. [[CrossRef](#)]
33. Li, L.; Feng, X.; Han, R.; Zang, S.; Yang, G. Cr(VI) removal via anion exchange on a silver-triazolate MOF. *J. Hazard. Mater.* **2017**, *321*, 622–628. [[CrossRef](#)]
34. Pei, Y.; Li, M.; Li, W.; Su, K.; Chen, J.; Yang, H.; Hu, D.; Zhang, S. Cr(VI) removal by cellulose-based composite adsorbent with a double-network structure. *Colloid Surface A* **2021**, *625*, 126963. [[CrossRef](#)]
35. Liu, W.; Jin, L.; Xu, J.; Liu, J.; Li, Y.; Zhou, P.; Wang, C.; Dahlgren, R.A.; Wang, X. Insight into pH dependent Cr(VI) removal with magnetic Fe₃S₄. *Chem. Eng. J.* **2019**, *359*, 564–571. [[CrossRef](#)]
36. Lu, S.; Hu, J.; Gao, Y.; Zhao, Y.; Ma, J. The removal mechanism of Cr(VI) by calcium titanate: Insight into the role of surface reduced Cr(III) in removal process. *Appl. Surf. Sci.* **2022**, *601*, 154235. [[CrossRef](#)]
37. Altun, T.; Kar, Y. Removal of Cr(VI) from aqueous solution by pyrolytic charcoals. *New Carbon Mater.* **2016**, *31*, 501–509. [[CrossRef](#)]
38. You, L.; Song, L.; Lu, F.; Zhang, Q. Fabrication of a copolymer flocculant and application for Cr(VI) removal. *Polym. Eng. Sci.* **2016**, *56*, 1213–1220. [[CrossRef](#)]
39. Yang, S.; Li, Q.; Chen, L.; Chen, Z.; Hu, B.; Wang, H.; Wang, X. Synergistic removal and reduction of U(VI) and Cr(VI) by Fe₃S₄ micro-crystal. *Chem. Eng. J.* **2020**, *385*, 123909. [[CrossRef](#)]
40. Zhang, D.; Liu, J.; Zhu, S.; Xiong, H.; Xu, Y. Adsorption removal of Cr(VI) by isomeric FeOOH. *Water Sci. Technol.* **2019**, *80*, 300–307. [[CrossRef](#)]
41. Shi, Y.J.; Zhang, T.; Ren, H.Q.; Kruse, A.; Cui, R.F. Polyethylene imine modified hydrochar adsorption for chromium (VI) and nickel (II) removal from aqueous solution. *Bioresour. Technol.* **2018**, *247*, 370–379. [[CrossRef](#)] [[PubMed](#)]
42. Zhou, L.; Liu, Y.G.; Liu, S.B.; Yin, Y.C.; Zeng, G.M.; Tan, X.F.; Hu, X.; Hu, X.J.; Jiang, L.H.; Liu, S.H.; et al. Investigation of the adsorption-reduction mechanisms of hexavalent chromium by ramie biochars of different pyrolytic temperatures. *Bioresour. Technol.* **2016**, *218*, 351–359. [[CrossRef](#)] [[PubMed](#)]
43. Zhang, H.; Xiao, R.; Li, R.; Ali, A.; Chen, A.; Zhang, Z. Enhanced aqueous Cr(VI) removal using chitosan-modified magnetic biochars derived from bamboo residues. *Chemosphere* **2020**, *261*, 127694. [[CrossRef](#)] [[PubMed](#)]
44. Saini, S.; Arora, S.; Kirandeep; Singh, B.P.; Katnoria, J.K.; Kaur, I. Nitrotriacetic acid modified bamboo charcoal (NTA-MBC): An effective adsorbent for the removal of Cr (III) and Cr (VI) from aqueous solution. *J. Environ. Chem. Eng.* **2018**, *6*, 2965–2974. [[CrossRef](#)]
45. Wang, W.; Wang, X.; Wang, X.; Yang, L.; Wu, Z.; Xia, S.; Zhao, J. Cr(VI) removal from aqueous solution with bamboo charcoal chemically modified by iron and cobalt with the assistance of microwave. *J. Chem. Sci.* **2013**, *25*, 1726–1735. [[CrossRef](#)] [[PubMed](#)]
46. Xue, X.; Yuan, W.; Zheng, Z.; Zhang, J.; Ao, C.; Zhao, J.; Wang, Q.; Zhang, W.; Lu, C. Iron-Loaded Carbon Aerogels Derived from Bamboo Cellulose Fibers as Efficient Adsorbents for Cr(VI) Removal. *Polymers* **2021**, *13*, 4338. [[CrossRef](#)] [[PubMed](#)]

Disclaimer/Publisher's Note: The statements, opinions and data contained in all publications are solely those of the individual author(s) and contributor(s) and not of MDPI and/or the editor(s). MDPI and/or the editor(s) disclaim responsibility for any injury to people or property resulting from any ideas, methods, instructions or products referred to in the content.